Nano Research 2015, 8(9): 2978–2987
DOI 10.1007/s12274-015-0803-1
Research Article
ISSN 1998-0124
CN 11-5974/O4

Nanoparticle monolayer-based flexible strain gauge with ultrafast dynamic response for acoustic vibration detection

Lizhi Yi[1], Weihong Jiao[1], Ke Wu[1], Lihua Qian[1] (✉), Xunxing Yu[2], Qi Xia[2], Kuanmin Mao[2], Songliu Yuan[1], Shuai Wang[3] (✉), and Yingtao Jiang[4]

[1] *School of Physics, Huazhong University of Science and Technology, Wuhan 430074, China*
[2] *School of Mechanical Science and Engineering, Huazhong University of Science and Technology, Wuhan 430074, China*
[3] *School of Chemistry and Chemical Engineering, Huazhong University of Science and Technology, Wuhan 430074, China*
[4] *Nevada Nanotechnology Center & Department of Electrical and Computer Engineering, University of Nevada, Las Vegas, Nevada 89154-4026, USA*

Received: 3 February 2015
Revised: 20 April 2015
Accepted: 23 April 2015

KEYWORDS
gold nanoparticle,
strain gauge,
self-assembly,
electron tunneling

ABSTRACT

The relatively poor dynamic response of current flexible strain gauges has prevented their wide adoption in portable electronics. In this work, we present a greatly improved flexible strain gauge, where one strip of Au nanoparticle (NP) monolayer assembled on a polyethylene terephthalate film is utilized as the active unit. The proposed flexible gauge is capable of responding to applied stimuli without detectable hysteresis via electron tunneling between adjacent nanoparticles within the Au NP monolayer. Based on experimental quantification of the time and frequency domain dependence of the electrical resistance of the proposed strain gauge, acoustic vibrations in the frequency range of 1 to 20,000 Hz could be reliably detected. In addition to being used to measure musical tone, audible speech, and creature vocalization, as demonstrated in this study, the ultrafast dynamic response of this flexible strain gauge can be used in a wide range of applications, including miniaturized vibratory sensors, safe entrance guard management systems, and ultrasensitive pressure sensors.

1 Introduction

With their active units made of hybrid architectures, flexible strain gauges have been found in numerous human and animal organs (e.g., human skin, cochlear hair, and the hearing and navigating systems of bats, elephants, dolphins, jellyfish, and rhinoceroses), enabling these organs to sensitively respond to mechanical vibrations in the wide frequency range of 5–150,000 Hz, spreading over the infrasonic, acoustic, and ultrasonic regions. Inspired by these naturally integrated systems, many flexible nanoarchitectures,

Address correspondence to Lihua Qian, lhqian@hust.edu.cn; Shuai Wang, chmsamuel@hust.edu.cn

including nanoparticle (NP) ensembles [1–3], nanowire/nanotube ensembles [4, 5], and three-dimensional graphene [6], have been configured into artificial gauges, which have now found niche applications in autonomous cars, industrial robots [7], electronic skin [8], wearable electronics, and portable devices [8]. In the literature, the fabrication of these man-made strain gauges has been demonstrated using innovative techniques and tools, including electron-beam lithography, self-assembly, chemical vapor deposition, and single electron tunneling [9, 10]. To a certain extent, these artificial nanoarchitectures, individually or collectively through their ensembles, mimic the functionalities of some natural organ counterparts, which helps the mechanical gauges to deliver the operating range of mechanical strain and signal reliability required by the applications. Individual VO_2 nanowires [11], monolayers of MoS_2 or graphene [12], and monolayers of NP [13] were observed to create a reversible electrical current or voltage signal due to piezoelectric or piezoresistive mechanisms, with superior detection limits. Monolayer MoS_2 was demonstrated to reproducibly sense mechanical strain as low as 0.53% [12]. Even more dramatically, a Au NP monolayer could convert mechanical strain as low as 0.0094% [13] into a reliable output signal based on electron tunneling events occurring within the nanoscale crevices. However, nanoarchitecture ensembles can simultaneously provide both desired reliability and a broad detection range beyond the elastic regime. The networks of carbon nanotubes and graphene [6], carbon-incorporated composites [14, 15], porous hydrogel/metal composites [16], metal/organic composites [17], and aligned rubber/metal core-shell nanowire [18] were experimentally demonstrated within a strain level reaching 300%. Normally, their high detection range intrinsically results from the overall number of contact points or area during mechanical loading/unloading.

In addition to the superior reliability and wide operation range of flexible strain gauges, the dynamic response is another challenging issue that impedes their application in precision devices. Most flexible strain gauges work in mechanical loading/unloading cycles with a frequency of only several Hz [4, 19]. Low dynamic responses limit the application of flexible strain gauges in some precision devices, such as acoustic and vibrating sensors. Indeed, the dynamic response of a flexible strain gauge is reflected in terms of duration that its contact point or area transforms from non-equilibrium to equilibrium states. Often, it takes a long time for a strain gauge consisting of complex nanoarchitectures to reach mechanical equilibrium, especially for three-dimensional ensembles.

2 Experimental

2.1 Fabrication and characterization of NP monolayer

According to a previous report [20], a strain gauge made from Au NP with a large diameter exhibited better sensitivity than one with a small diameter. Systematic investigations concluded that a 15-fold enhancement in sensitivity was observed with an increase in diameter from 15 to 97 nm. Both the detection limit and gauge factor also exhibited a similar dependence on NP size. Thus, Au NP with a diameter of 100 nm was selected as the building block for the convective assembly and configuration of the strain gauge in our investigation. Urchin-like Au NPs with diameters of 100 nm were synthesized by seed-mediated reduction of gold (III) chloride trihydrate ($HAuCl_4$). The cetyltrimethyl ammonium bromide (CTAB) molecule was utilized as a surfactant to avoid the aggregation of Au NPs during chemical synthesis. The details on the NP synthesis were well documented in our previous investigation [21]. The original Au colloid was centrifuged two times to remove most residual chemicals. In this case, traces of CTAB molecules remained on the NP surfaces, such that the colloid with the well-dispersed NP could be attained for convective assembly. To obtain the well-defined pattern of the NP monolayer, the polyethylene terephthalate (PET) film was treated by ultrasonic cleaning in water and ethanol to remove tiny dust. After this treatment, no additional functional groups were introduced onto the substrate surface; therefore, the interaction between the Au NPs and PET substrate was most likely a Van der Waals force. The geometry of the flexible PET substrate supporting the NP monolayer was 40 mm × 10 mm × 0.09 mm. The procedure

to assemble NP strip with a width of 2–3 μm was described in our previous work [13]. Au NPs were dispersed onto an amorphous C film supported by a Cu grid for transmission electron microscopy (TEM) observations. All the NPs had urchin-like surface contours, and the average particle size was statistically estimated to be ~100 nm.

2.2 Mechano-electrical characterization of strain gauge

The NP monolayer was assembled onto the flexible PET film with a scale of 2–3 μm × 8 mm. A metal wire with a diameter of ~90 μm was utilized as a mask covering the NP line vertically. Stencil lithography was applied to deposit Au electrodes that were ~90 μm apart using thermal evaporation. Temperature elevation might induce random contractions of the flexible substrate during electrode fabrication. In our experiments, the PET substrate potentially retained geometrical stability at high deposition temperature compared with flexible polyethylene (PE) and polydimethylsiloxane (PDMS) substrates. The NP monolayer assembled onto the PET film laid horizontally during the measurement. One terminal was immobilized; the other terminal was driven by a vibration executor driven by a function generator that was tunable over a frequency range of 1–20,000 Hz. The strain gauge was connected in series with a divider resistance. The voltage between the two terminals of the divider resistor was collected using an NI data acquisition card (DAQ).

2.3 Real-time measurement of mechanical displacement

During the bending of the strain gauge, the horizontal displacement of the mobile end was recorded using a Keyence LK-G80 digital laser rangefinder (DLR). The bending radius of the PET substrate was calculated using the horizontal displacement and initial length. The strain ε induced in the NP monolayer was calculated using $\varepsilon = t/2r$, where t is the thickness of the PET substrate and r is its curvature after mechanical bending. For the details of the calculation, refer to Ref. [22].

3 Results

3.1 Quasi-static performance of NP-based strain gauge

In this study, however, we experimentally demonstrate that a NP monolayer assembled onto a flexible substrate can promptly adjust the interparticle gap during mechanical bending, leading to an ultrafast dynamic response that accommodates acoustic vibrations with a range of 1–20,000 Hz.

Au NPs convection toward the contact line and their self-organization into ordered arrays can be simultaneously triggered by solvent evaporation [19], which is widely utilized to create well-defined linear arrays consisting of microspheres, NPs [23], and even quantum dots [24]. In our previous investigation, convective assembly at the confined contact angle was developed to synthesize a uniform monolayer of Au NPs [13], and the operating principle of this technique is schematically illustrated in Fig. 1(a). The yellow line in Fig. 1(b) was visible using an optical microscope because of the strong scattering of the Au NPs with urchin-like surface contours (see TEM image

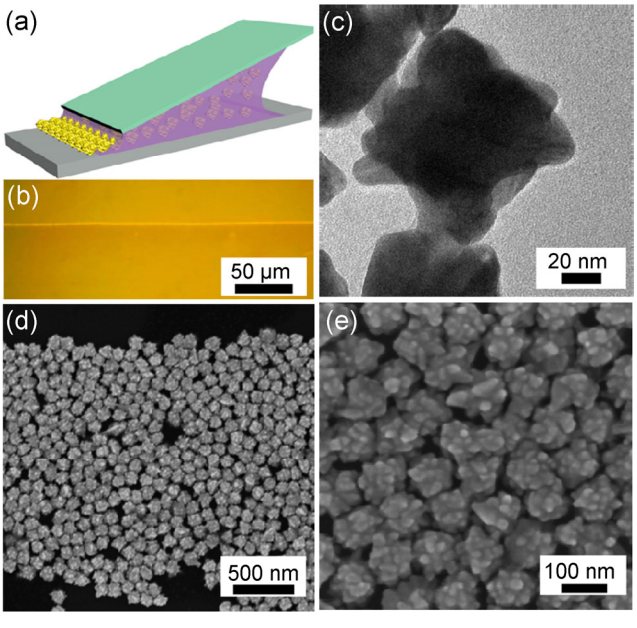

Figure 1 Au NP monolayer prepared using convective assembly. (a) Schematic illustration of the assembly of one strip of Au NPs. (b) Optical micrograph of NP strip (yellow line). (c) TEM image of Au NPs with rough surfaces. (d) and (e) SEM images of NP monolayer with a width of 2–3 μm.

in Fig. 1(c)) with incident light. The planar arrangement of Au NPs with a size of ~100 nm could be further characterized using scanning electron microscopy (SEM). It is clear that a single layer of Au NPs is assembled on the substrate. Most NPs, as shown in Fig. 1(d), are closely packed in two dimensions. In Fig. 1(d), one can see some vacancy defects in the NP monolayer, and the formation of these defects might stem from the geometrical confinement of surface protrusions because of the disturbing convection and organization of Au NPs near the contact line during the self-assembly. The magnified SEM image in Fig. 1(e) reveals that most of the NPs almost physically touch their respective neighboring NPs, and some tiny crevices can be observed because of the disturbing effect of nanoscale protrusions onto the NP surfaces.

One strip of NP monolayer assembled onto the flexible PET was utilized as the active unit of the strain gauge. Two Au electrodes were discretely deposited onto the two ends of the strip for electrical characterization. One end was immobilized, and the other end was motorized by translation stages or a vibration exciter for precise control of the mechanical strain. The PET film lying horizontally might exhibit convex and concave profiles during mechanical bending, corresponding to tensile and compressive strains for the top surface, respectively. The strain assumes a positive value in the tensile state, and a negative value in the compressive state. The current–voltage (*I*–*V*) characteristics in compressive, unstrained, and tensile states are shown in Fig. 2(a). Of these three states, the transient variation of electrical current shows a perfect linear relationship with respect to the voltage sweeping from −2 to 2 V. The slope in the compressive state is larger than those in the unstrained and tensile states, suggesting that electron tunneling between adjacent NPs tends to occur when their interparticle gaps are shrunk. With the conformal covering of the PET film onto the cylinders with different diameters, the mechanical strain or the interparticle separation can then be precisely calculated and tailored. The minimum detectable mechanical strain is as low as 0.03%, which is comparable to that of a flexible gauge consisting of monolayer NPs with smooth surface contours (see Fig. S1 in the Electronic Supplementary Material (ESM)) [13]. To determine the intrinsic mechanism for strain sensing, the relative resistance change as a function of mechanical strain is presented in Fig. 2(b). According to quantum tunneling theory, the electrical resistance of metallic NP arrays can be described as [25]

$$R \propto e^{\beta d} \tag{1}$$

where d is the interparticle distance and β is the electron coupling term determined by the particle size and ambient temperature. When the interparticle distance shifts from d to $d + \Delta d$, the mechanical strain can be estimated as $\varepsilon = \Delta d/d$. Therefore

$$\frac{\Delta R}{R} \propto e^{\beta d} - 1 = e^{\beta d\varepsilon} - 1 \tag{2}$$

It is clear that the $\Delta R/R$~ε relation should be

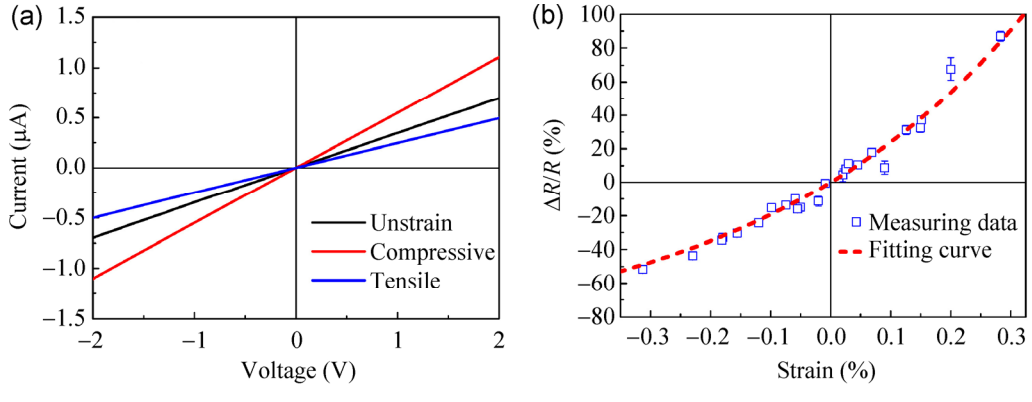

Figure 2 Quasi-static performance of NP-based strain gauge. (a) Variation of electrical current with the supplied voltage in three different states (compressive, unstrained, and tensile). (b) $\Delta R/R$ as a function of mechanical strain. The blue square is the measurement data, and the red dotted line is the fitting curve according to Eq. (2).

established for Eq. (2). The correlation between the experimental data and theoretical model in Fig. 2(b) is a clear indicator that the intrinsic mechanism of strain sensing relates to electron tunneling between the adjacent NPs, which is in sound agreement with the results reported in an early study [26].

According to our previous investigations, mechanical stimulus of the NP monolayer can be accurately tracked by measuring the electrical signal output [13]. The relationship between the mechanical strain and electrical transport of the gauge is shown in Fig. S2 (in the ESM). Note that the electrical resistance of NP monolayer can rapidly track the periodic vibration of the PET film without introducing noticeable signal hysteresis. Such a prompt response in electrical resistance is the result of an instantaneous change and recovery of the interparticle gaps when mechanical stimulus is periodically applied to the PET film, making it possible to detect mechanical loading/unloading at a higher frequency by examining electrical transport across the NP monolayer.

3.2 Dynamic sensing performance of Au NP monolayer

To determine the dynamic response of flexible NP monolayers, the electrical resistance was recorded when mechanical strains were alternatively loaded and unloaded with frequencies varying from 1–20,000 Hz. Figure 3(a) shows the layout of an instrument that was built in-house that includes a vibration–excitation module, electrical circuit kit, and data acquisition component. The vibration exciter, which is controlled by a function generator, can exert mechanical strain with a desired frequency onto the NP-based gauge. The data acquisition board outputs the differential voltage of the gauge, which is then translated by software into electrical resistance, considering the geometrical parameter of the NP monolayer.

When mechanical stimuli with the loading–unloading frequencies of 500 and 1,000 Hz are applied, the temporal response of electrical resistance, shown in Figs. 3(b) and 3(c), shows resistance without any noticeable background drift. From the resistance variation over a time interval of 100–120 ms magnified from Fig. 3(c), one can see that the electrical resistance (in Fig. 3(d)) is a reliable measure of the alternative switching of compressive strain. In general, the gauge developed here can simultaneously detect the periodical mechanical stimulus with a vibration frequency up to 20,000 Hz (see Fig. 3(e) and Fig. S3 in the ESM). Figure 3(f) shows $\Delta R/R$ with respect to mechanical strain at two different equilibrium positions: $\varepsilon = -0.21\%$ and -0.1%. The $\Delta R/R$–ε relationship in the dynamic experiments follows a similar trend to that in the quasi-static state. Such a fast dynamic response to mechanical stimulus and the coherence between the static and dynamic output signals allows this flexible gauge to detect acoustic vibrations.

3.3 Dynamic response of NP monolayer to musical tones and sound

To examine the capability of the NP-based gauge to sense acoustic vibration at higher frequency, three types of vibration, musical tones, audible speech, and creature vocalization, were selected as excitation sources. Figure 4(a) shows the electrical resistances recorded by the NP-based gauge, corresponding to seven pure high-pitched notes, namely Do, Re, Mi, Fa, Sol, La, and Si. The electrical resistance generated by the gauge oscillates in a periodic fashion, and its amplitude slowly decays over time; all the tones have waveforms similar to their respective original sources. One great advantage of the NP-based gauge over most flexible strain gauges is that in addition to the waveform, it can provide an additional piece of information, the frequency of the vibrator. As observed in Fig. 4(b), the waveform corresponding to the tone Re shows the same frequency between the output and input signals; each tone can be reliably identified by estimating its characteristic frequency. The detected frequencies for the high-pitched tones Do, Re, Mi, Fa, Sol, La, and Si, are 525, 590, 663, 703, 789, 887, and 995 Hz, respectively. All the vibrator frequencies and their corresponding tones are shown in Fig. 4(c). The perfect match between the input and output signals demonstrates that the gauge is able to reliably track the frequencies of the pure tones. Our experiment indicated that the exact frequencies of the middle-pitched and low-pitched tones can also be reliably detected by measuring the temporal electrical resistances, as shown in Fig. S4 (in the ESM). The frequency range spans 132 to 496 Hz when the source tones go

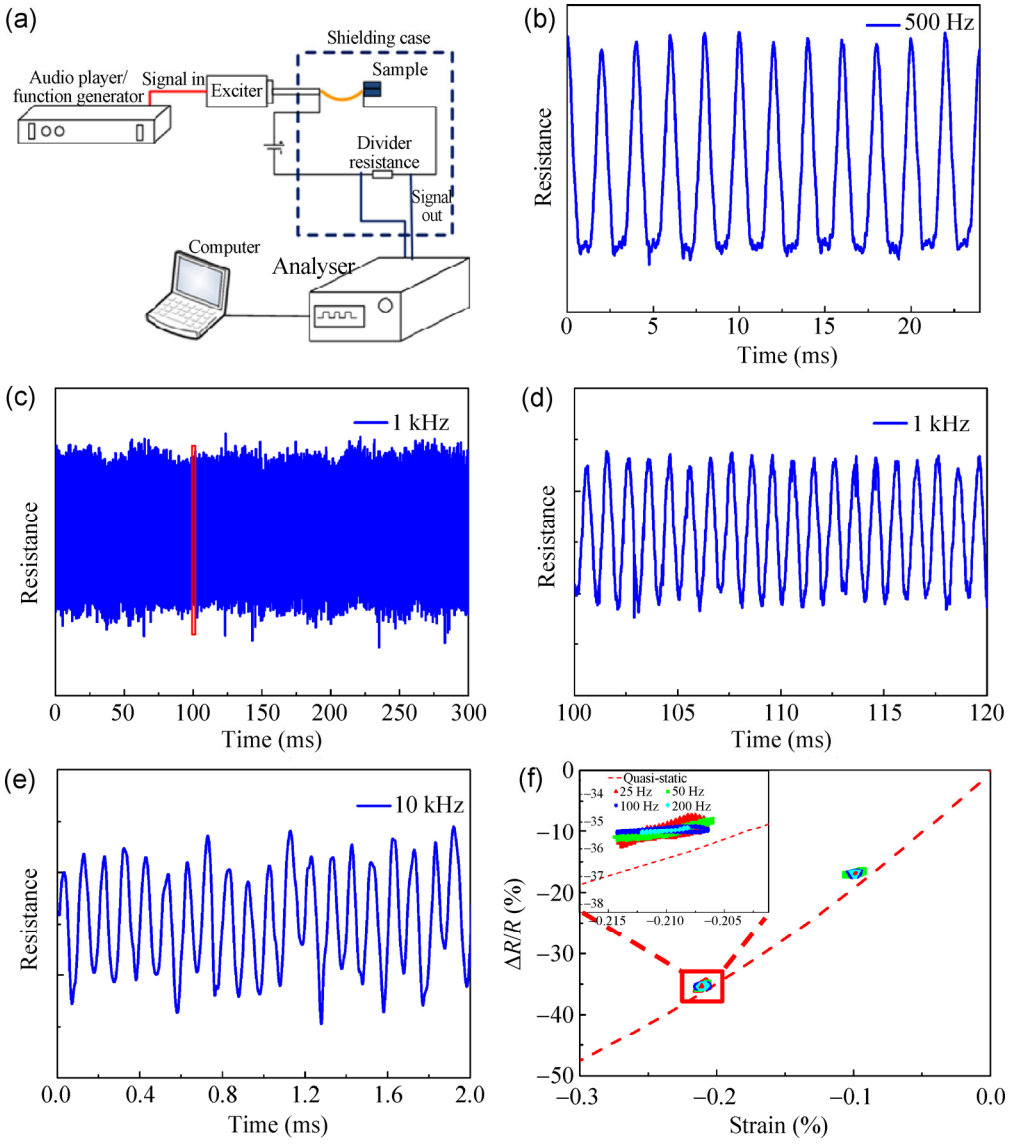

Figure 3 Dynamic sensing performance of Au NP monolayer. (a) Schematic illustration of experimental setup for electrical property measurement at high frequency. (b)–(e) Temporal response of electrical resistance at various frequencies of 500–10,000 Hz. (f) Coherent verification of $\Delta R/R$–ε relations in quasi-static state (red dotted line) and two typical dynamic states with different levels of pre-strains in compressive states.

from the low-pitched Do to middle-pitched Si. The reliable signal outputs to pure tone inputs makes the gauge particularly appreciated in music applications. Piano music of the famous song "Yesterday once more" with complex melodies was utilized as an example to detect acoustic vibration. The reliable detection of acoustic vibrations was also accomplished (Fig. 4(d)) by collecting electrical resistance of the NP-based gauge developed in this work. The song "Happy birthday to you" consisting of various pure tones was successfully detected by employing this NP-based gauge, and their frequencies were reproducibly estimated, as illustrated in Fig. S5 (in the ESM). Note that the output signal generated by the gauge is a playback of the original music or tones with extremely high fidelity, as documented in the ESM for all the audio files. Although the quality of the melodies is slightly lower than that of the original music, further optimization of the detecting sensitivity in the NP monolayer arrays should help improve the sound quality in the future.

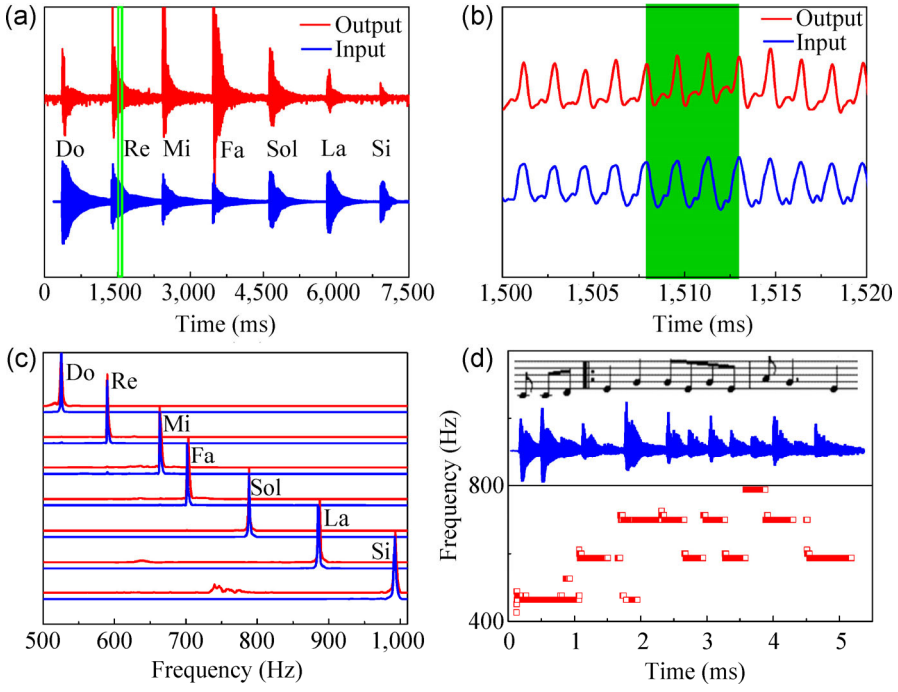

Figure 4 Dynamic response of NP monolayer to musical tones and a music clip from "Yesterday once more" and analysis of their vibratory frequencies. (a) Waveform of seven high-pitched tones detected by the NP monolayer. (b) The magnified waveform of pure tones corresponding to high-pitched "Re". (c) Frequency analysis of these seven pure tones. All the red lines were determined from electrical signals exported from the NP monolayer, and the blue lines are the input signals. (d) Waveform of a music clip from "Yesterday once more" and its frequency analysis.

To further demonstrate the superior ability of the gauge to sense acoustic vibrations with more complicated frequency components, the famous "I have a dream" speech delivered by Dr. Martin Luther King Jr. and several creature vocalizations were also selected as source signals. Figure 5(a) shows the electrical resistances with respect to the four clipped sentences recorded at intervals of 16", 43", 59", and 97" (referring to the input and output audios in the ESM). For the repeated phrase of "I have a dream", the electrical resistances differ considerably from each other because of the time domain dependence. Most valuably, the frequency domain dependence of the electrical resistance can clearly distinguish the detailed frequency and its distribution for each word (Fig. 5(b)). In addition, the significantly different frequencies of the words "have" and "dream" are distinguishable in the phase at 97" compared with the others. Detailed comparisons between the source audio and output audio obtained from the NP-based gauge are included in the ESM. Compared with the human voice frequency range (60–1,000 Hz), some creatures have a wider register. Figure 5(c) shows the frequency spectrum of various creatures' voices detected by the NP-based gauge. One can see in Fig. 5(c) that the highest frequency of the redbreast's voice is approximately 4,000 Hz.

4 Discussion

As described above, the advantage of the NP-based strain gauge is its reliable detection of acoustic vibrations at frequencies as high as 20,000 Hz because of the ultrafast dynamic response of its electrical resistance to external stimulus. Many intrinsic factors relating to the active unit and extrinsic factors relating to the measuring parameters contribute to this fast dynamic response. Essentially, the sensing mechanism depends on the tunable electrical resistance within the monolayer of Au NPs residing on the flexible PET film. Microstructural characterization revealed that most crevices between neighboring NPs are in the range of several nanometers, as observed in Fig. 1,

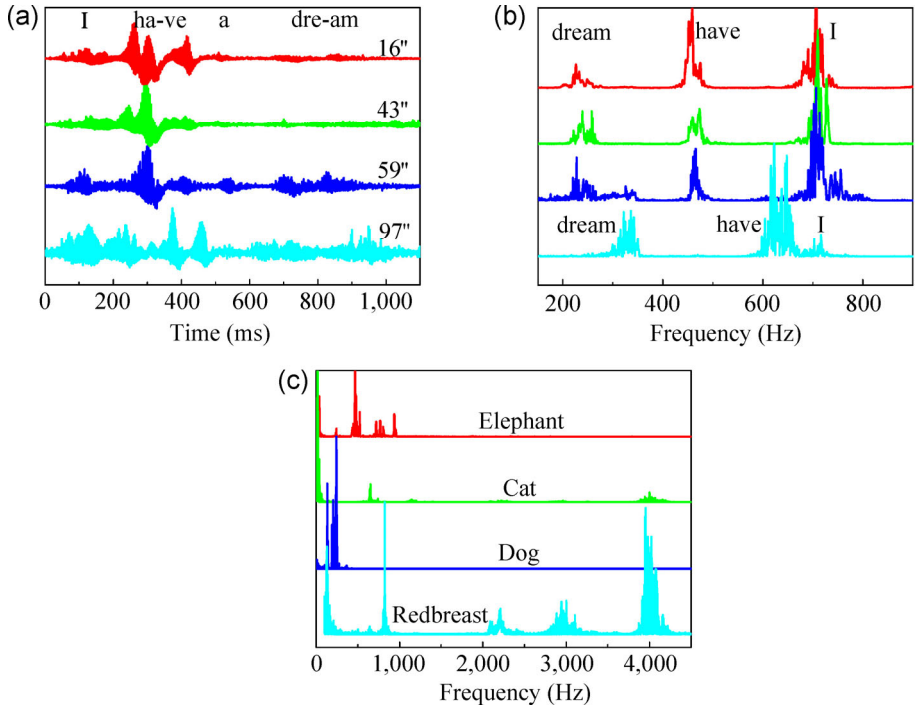

Figure 5 Dynamic response of NP monolayer to famous "I have a dream" speech and creature vocalizations. (a) Temporal changes of electrical resistances corresponding to the four clipped segments at different nodes of the "I have a dream" speech, demonstrating the distinct time-domain dependences of the electrical resistance. (b) Frequency analysis of various clipped segments of "I have a dream", demonstrating the distinct frequency-domain dependences of the electrical resistance. (c) Frequency analysis of various creature vocalizations.

and in some regions, neighboring NPs may actually touch each other. The steady current/or resistance can be obtained in dual measuring configurations, including *I*–*V* sweeping and the temporal change of the electrical resistance at different straining states. The linear *I*–*V* curve within a range of –2 to 2 V indicates that the electrons involve transport within a unit volume located in the ohmic region. In this case, the magnitude of the electrical current only depends on the drifting velocities of free electrons at the bias voltage, regardless of tunneling electrons or the electrons across the junction between the contacting NPs. However, when the PET film vibrates, one possible contribution to electrical resistance is the effective number of contact points or areas. However, the entire number of free electrons across these contacting junctions appears to be random rather than follow exponential relations. In particular, the $\Delta R/R$–ε relation with an exponential dependence actually confirms that electron tunneling is the dominant factor in the detection of mechanical strain.

As the electrical resistance is sensitive to the crevice size in electron tunneling, the NP-based strain gauge outperforms the other types of flexible gauges in terms of the gauge factor (*G*), detection limit, and dynamic response of the electrical signal to external stimulus. For of the monolayer Au NPs with urchin-like surface contours in this work, *G*, which is defined as the ratio between the relative resistance change and mechanical strain, can approach 300 (calculated from Fig. 2(b)), which is much higher than that of metal spheres with smooth surfaces (see Table S1 in the ESM). The much improved *G* value might result from the tunneling probability of the electrons following an exponential rather than linear dependence. In addition, an important advantage of the NP-based strain gauge is its relatively low detection limit, which is comparable to that of conventional Si-based semiconductor gauges [27] and much better than that of carbon-incorporated or organic materials [28]. In this work, the lowest strain to be measured was ~0.03%, which is comparable to that of previous reports [23], implying the promising

merit of the finely tunable electron tunneling for precise sensing of mechanical stimulus in the miniaturized stain gauge. Another figure of merit is the response time of the strain gauge, one of the important factors affecting its dynamic performance. Figure S2 in the ESM shows the exact matching between the mechanical displacement and electrical output during acoustic vibration, implying that electron tunneling between the adjacent NPs can be tuned with any hysteresis in the working frequency investigated here. The ultrafast response of electrical resistance to external stimulus with high frequency might result from the well-defined arrangement of Au NPs onto the PET film through convective assembly. Each NP is so tightly attached to the flexible substrate that a NP can experience both tensile and compressive strains without noticeable hysteresis. Although some defects are really embedded within the NP monolayer, as observed in Fig. 1(d), the planar fraction of these defects can be estimated to be as small as 1%. However, the active unit for the strain gauge nearly consists of more than 18,000 NPs, such that many nanoscale crevices can involve electron tunneling even if some defects can be found in the NP monolayer. The tunneling events can occur in numerous nanoscale crevices, which actually imply that this small fraction of defects will not affect the sensing performance of the strain gauge. In addition, because the mechanical strain applied in this work is within the elastic range, it is impossible to squeeze out any NPs within the arrays, even those NPs that are physically in contact with each other, during the PET bending. Therefore, electron tunneling between the adjacent NPs can simultaneously track the evolution of the interparticle distance when the PET film is vibrating with a constant frequency.

5 Conclusions

In summary, a monolayer of Au NPs assembled on a flexible substrate was configured as a strain gauge with a low detection limit of 0.03% and a large gauge factor of 300. The tunneling current between the adjacent NPs results in an ultrafast dynamic response to external stimulus without detectable hysteresis. This result occurs because of the almost synchronic tunability of the interparticle gap, such that the time and frequency domain dependence of the electrical resistance for reliable detection can monitor acoustic vibrations with a frequency range of 1–20,000 Hz. Consequently, pure musical tones with constant frequency, audible speech, and creature vocalization with complex frequency components can be reliably and precisely identified. The ultrafast dynamic response reported in this work would allow the proposed flexible strain gauge to be used to build miniaturized vibration sensors, safe entrance guard management systems, and ultrasensitive pressure sensors.

Acknowledgements

This work was partially supported by Innovation Funding of HUST for International Collaborations (No. 2014ZZGH018), Specialized Research Fund for the Doctoral Program of Higher Education (No. 20130142120089), and the National Natural Science Foundation of China (No. 51371084 and 51173055).

Electronic Supplementary Material: Supplementary material (the supporting figures, tables and audio files) is available in the online version of this article at http://dx.doi.org/ 10.1007/s12274-015-0803-1.

References

[1] Guédon, C. M.; Zonneveld, J.; Valkenier, H.; Hummelen, J. C.; van der Molen, S. J. Controlling the interparticle distance in a 2D molecule-nanoparticle network. *Nanotech*. **2011**, *22*, 125205–125209.

[2] Kim, Y.; Zhu, J.; Yeom, B.; Di Prima, M; Su, X. L.; Kim, J. G.; Yoo, S. J.; Uher, C.; Kotov, N. A. Stretchable nanoparticle conductors with self-organized conductive pathways. *Nature* **2013**, *500*, 59–64.

[3] Takei, K.; Yu, Z. B.; Zheng, M.; Ota, H.; Takahashi, T.; Javey, A. Highly sensitive electronic whiskers based on patterned carbon nanotube and silver nanoparticle composite films. *Proc. Natl. Acad. Sci. USA* **2014**, *111*, 1703–1707.

[4] Yao, S. S.; Zhu, Y. Wearable multifunctional sensors using printed stretchable conductors made of silver nanowires. *Nanoscale* **2014,** *6*, 2345–2352.

[5] Gong, S.; Schwalb, W.; Wang, Y. W.; Chen, Y.; Tang, Y.; Si, J.; Shirinzadeh, B.; Cheng, W. L. A wearable and highly sensitive pressure sensor with ultrathin gold nanowires. *Nat. Commun*. **2014**, *5*, 3132–3139.

[6] Chen, Z. P.; Ren, W. C.; Gao, L. B.; Liu, B. L.; Pei, S. F.; Cheng, H. M. Three-dimensional flexible and conductive interconnected graphene networks grown by chemical vapour deposition. *Nat. Mater*. **2011**, *10*, 424–428.

[7] Tee, B. C.-K. T.; Wang, C.; Allen, R.; Bao, Z. N. An electrically and mechanically self-healing composite with pressure- and flexion-sensitive properties for electronic skin applications. *Nat. Nanotechnol.* **2012**, *7*, 825–832.

[8] Wang, X. W.; Gu, Y.; Xiong, Z. P.; Zheng, C.; Zhang, T. Silk-molded flexible, ultrasensitive, and highly stable electronic skin for monitoring human physiological signals. *Adv. Mater.* **2014**, *26*, 1336–1342.

[9] Segev-Bar, M.; Haick, H. Flexible sensors based on nanoparticles. *ACS Nano* **2013**, *7*, 8366–8378.

[10] Kane, J.; Ong, J.; Saraf, R. F. Chemistry, physics, and engineering of electrically percolating arrays of nanoparticles: A mini review. *J. Mater. Chem*. **2011**, *21*, 16846–16858.

[11] Hu, B.; Zhang, Y.; Chen, W.; Xu, C.; Wang, Z. L. Self-heating and external strain coupling induced phase transition of VO_2 nanobeam as single domain switch. *Adv. Mater.* **2011**, *23*, 3536–3541.

[12] Wu, W. Z; Wang, L.; Li, Y. L.; Zhang, F.; Lin, L.; Niu, S. M.; Chenet, D.; Zhang, X.; Hao, Y. F.; Heinz, T. F. et al. Piezoelectricity of single-atomic-layer MoS_2 for energy conversion and piezotronics. *Nature* **2014**, *514*, 470–474.

[13] Jiao, W. H.; Yi, L. Z.; Zhang, C.; Wu, K.; Li, J.; Qian, L. H.; Wang, S.; Jiang, Y. T.; Das, B.; Yuan, S. L. Electrical conduction of nanoparticle monolayer for accurate tracking of mechanical stimulus in finger touch sensing. *Nanoscale* **2014**, *6*, 13809–13816.

[14] Cai, L.; Song, L.; Luan, P. S.; Zhang, Q.; Zhang, N.; Gao, Q. Q.; Zhao, D.; Zhang, X.; Tu, M.; Yang, F. et al. Super-stretchable, transparent carbon nanotube-based capacitive strain sensors for human motion detection. *Sci. Rep.* **2013**, *3*, 3048–3055.

[15] Li, X .; Zhang, R. J.; Yu, W. J.; Wang, K. L.; Wei, J. Q.; Wu, D. H.; Cao, A. Y.; Li, Z. H.; Cheng, Y.; Zheng, Q. S. et al. Stretchable and highly sensitive graphene-on-polymer strain sensors. *Sci. Rep.* **2012**, *2*, 870–875.

[16] Pan, L. J.; Chortos, A.; Yu, G. H.; Wang, Y. Q.; Isaacson, S.; Allen, R.; Shi, Y.; Dauskardt, R.; Bao, Z. N. An ultra-sensitive resistive pressure sensor based on hollow-sphere microstructure induced elasticity in conducting polymer film. *Nat. Commun.* **2014**, *5*, 3002–3009.

[17] Takei, K.; Takahashi, T.; Ho, J. C.; Ko, H.; Gillies, A. G.; Leu, P. W.; Fearing, R. S.; Javey, A. Nanowire active-matrix circuitry for low-voltage microscale artificial skin. *Nat. Mater.* **2010**, *9*, 821–826.

[18] Pang, C.; Lee, G. Y.; Kim, T. I.; Kim, S. M.; Kim, H. N.; Ahn, S. H.; Suh, K. Y. A flexible and highly sensitive strain-gauge sensor using reversible interlocking of nanofibres. *Nat. Mater.* **2012**, *11*, 795–801.

[19] Trung, T. Q.; Tien, N. T.; Kim, D.; Jang, M.; Yoon, O. J.; Lee, N. E. A flexible reduced graphene oxide field-effect transistor for ultrasensitive strain sensing. *Adv. Funct. Mater.* **2014**, *24*, 117–124.

[20] Sangeetha, N. M.; Decorde, N.; Viallet, B.; Viau, G.; Ressler, L. Nanoparticle-based strain gauges fabricated by convective self assembly: Strain sensitivity and hysteresis with respect to nanoparticle sizes. *J. Phys. Chem. C* **2013**, *117*, 1935–1940.

[21] Wu, K.; Zhang, J. P.; Fan, S. S.; Li, J.; Zhang, C.; Qiao, K. K.; Qian, L. H.; Han, J. B.; Tang, J.; Wang, S. Plasmon-enhanced fluorescence of PbS quantum dots for remote near-infrared imaging. *Chem. Commun.* **2015**, *51*, 141–144.

[22] Hempel, M.; Nezich, D.; Kong, J.; Hofmann, M. A novel class of strain gauges based on layered percolative films of 2D materials. *Nano Lett*. **2012**, *12*, 5714–5718.

[23] Zhang, C.; Li, J.; Yang, S. S.; Jiao, W. H.; Xiao, S.; Zou, M. Q.; Yuan, S. L.; Xiao, F.; Wang, S.; Qian, L. H. Closely packed nanoparticle monolayer as strain gauge fabricated by convective assembly at the confined angle. *Nano Res.* **2014**, *7*, 824–834.

[24] Hong, S. W.; Byun, M.; Lin, Z. Q. Robust self-assembly of highly ordered complex structures by controlled evaporation of confined microfluids. *Angew. Chem., Int. Ed*. **2009**, *48*, 512–516.

[25] Herrmann, J.; Muller, K. H.; Reda, T.; Baxter, G. R.; Raguse, B.; de Groot, G. J. J. B.; Chai, R.; Roberts, M.; Wieczorek, L. Nanoparticle films as sensitive strain gauges. *Appl. Phys. Lett.* **2007**, *91*, 1831051–1831053.

[26] Simmons, J. G. Generalized formula for the electric tunnel effect between similar electrodes separated by a thin insulating film. *J. Appl. Phys.* **1963**, *34*, 1793–1803.

[27] Smith, C. S. Piezoresistance effect in germanium and silicon. *Phys. Rev*. **1954**, *94*, 42.

[28] Bae, S. H.; Lee, Y.; Sharma, B. K.; Lee, H. J.; Kim, J. H.; Ahn, J. H. Graphene-based transparent strain sensor. *Carbon* **2013**, *51*, 236–242.